

The proteasomal subunit Rpn6 is a molecular clamp holding the core and regulatory subcomplexes together

Ganesh Ramnath Pathare^a, István Nagy^a, Stefan Bohn^a, Pia Unverdorben^a, Agnes Hubert^a, Roman Körner^b, Stephan Nickell^a, Keren Lasker^{c,d}, Andrej Salic^c, Tomohiro Tamura^{e,f}, Taiki Nishioka^f, Friedrich Förster^a, Wolfgang Baumeister^{a,1}, and Andreas Bracher^{b,1}

^aDepartment of Molecular Structural Biology, Max-Planck-Institute of Biochemistry, Am Klopferspitz 18, 82152 Martinsried, Germany; ^bDepartment of Cellular Biochemistry, Max-Planck-Institute of Biochemistry, Am Klopferspitz 18, 82152 Martinsried, Germany; ^cLaboratory of Molecular Environmental Microbiology, Graduate School of Agriculture, Hokkaido University, Kita-9, Nishi-9, Kita-ku, Sapporo 060-8589, Japan; ^dDepartment of Bioengineering and Therapeutic Sciences, Department of Pharmaceutical Chemistry, and California Institute of Quantitative Biosciences, 1700 4th Street, University of California, San Francisco, CA 94158; ^eBlavatnik School of Computer Science, Raymond and Beverly Sackler Faculty of Exact Sciences, Tel Aviv University, Tel Aviv 69978, Israel; and ^fBioproduction Research Institute, National Institute of Advanced Industrial Science and Technology (AIST), 2-17-2-1, Tsukisamu-Higashi, Toyohira-ku, Sapporo 062-8517, Japan

Contributed by Wolfgang Baumeister, October 26, 2011 (sent for review August 4, 2011)

Proteasomes execute the degradation of most cellular proteins. Although the 20S core particle (CP) has been studied in great detail, the structure of the 19S regulatory particle (RP), which prepares ubiquitylated substrates for degradation, has remained elusive. Here, we report the crystal structure of one of the RP subunits, Rpn6, and we describe its integration into the cryo-EM density map of the 26S holocomplex at 9.1 Å resolution. Rpn6 consists of an α -solenoid-like fold and a proteasome COP9/signalosome eIF3 (PCI) module in a right-handed suprahelical configuration. Highly conserved surface areas of Rpn6 interact with the conserved surfaces of the Pre8 (α 2) and Rpt6 subunits from the α and ATPase rings, respectively. The structure suggests that Rpn6 has a pivotal role in stabilizing the otherwise weak interaction between the CP and the RP.

26S proteasome | cryoelectron microscopy | PSMD11 | S9 | PCI domain

Protein degradation is of vital importance for the maintenance of protein homeostasis, for the removal of misfolded proteins, and for the control of numerous regulatory processes (1, 2). In eukaryotic cells, the main pathway for protein degradation is the ubiquitin-proteasome system (3). It has the capability of degrading almost any protein, and yet it acts with exquisite specificity. The ubiquitin system selects proteins and marks them for destruction, whereas the 26S proteasome is the executioner of proteolysis. Malfunctions of the system have been implicated in a variety of diseases (2).

The 26S proteasome is a molecular machine of approximately 2.5 MDa built from two copies each of 34 canonical subunits and several proteasome interacting proteins, which are present in substoichiometric amounts (4–6). The 26S holocomplex comprises two subcomplexes: The barrel-shaped core particle (CP) that harbors the proteolytically active sites and sequesters them from the cellular environment, and the regulatory particles (RPs) that bind to one or both ends of the CP. Their role is to prepare substrates for degradation; this preparation includes the recognition of polyubiquitylated proteins, their deubiquitylation and unfolding and, eventually, assistance in their translocation into the CP through the gate in the α -ring of the CP.

The CP, which is a stack of four seven-membered rings (α 1–7; β 1–7; β 1–7; α 1–7), is structurally well characterized; it is highly conserved from archaea to mammals, and crystal structures are available for CPs from several species (7–9). In contrast to the CP, the structure of the RP is only dimly understood. So far, all attempts to crystallize the RP alone or in association with the CP have been unsuccessful. Recently, EM single particle analysis has provided a map of the 26S holocomplex at medium resolution

(9.1 Å), which provides a platform for the integration of high-resolution structures of the constituent subunits (10).

The RP is composed of a core of 19 different subunits, which can dissociate into a “base” and a “lid” subcomplex (11). The base is thought to form the proximal part of the RP, which associates with the α -rings of the CP, whereas the lid forms the distal end. The base comprises a heterohexameric AAA-ATPase module (Rpt1–Rpt6) and the non-ATPase subunits Rpn1 and Rpn2 (11). The often substoichiometric subunits Rpn10 and Rpn13 are also commonly assigned to the base subcomplex (5). The lid part of the RP is composed of the Rpn3, Rpn5–Rpn9, and Rpn11–Rpn12 subunits (11). The lid subunits can be classified into two groups according to their predicted domain structure: Rpn3, Rpn5, Rpn6, Rpn7, Rpn9, and Rpn12 are predicted to share a C-terminal module present in proteasome, COP9/signalosome, and eIF3 subunits (PCI module), whereas Rpn8 and Rpn11 subunits have an MPN (Mpr1, Pad1 N-terminal) domain in common (12). Functionally, Rpn10 and Rpn13 serve as polyubiquitin receptors, whereas Rpn11 has deubiquitylation activity (4, 5). The PCI module was proposed to have a structural role and is composed of an N-terminal helix bundle and a winged-helix subdomain (13–15).

The PCI subunit Rpn6 was found to be an essential component of the 26S proteasome in *Saccharomyces cerevisiae* (16), *Trypanosoma brucei* (17), *Plasmodium falciparum* (18), and *Drosophila melanogaster* (19). Upon conditional knock-out in *S. cerevisiae*, only partially assembled complexes lacking all the lid subunits were found, and the cells were arrested in G2/M phase (20). Similarly, a temperature-sensitive Rpn6 mutant strain of *S. cerevisiae* yielded only partially assembled complexes at the restrictive temperature, suggesting a critical role of Rpn6 for assembly (21).

Here, we present the crystal structure of Rpn6 from *D. melanogaster*. The distinctive shape of this subunit and the prevalence of α -helices allowed us to fit the structure into the 9.1 Å cryo-EM map of the 26S proteasome of *Schizosaccharomyces pombe* with high confidence. The hybrid structure reveals highly conserved

Author contributions: A.S., F.F., W.B., and A.B. designed research; G.R.P., I.N., S.B., A.H., R.K., T.T., T.N., and A.B. performed research; G.R.P., P.U., S.N., K.L., F.F., and A.B. analyzed data; and G.R.P., A.S., F.F., W.B., and A.B. wrote the paper.

The authors declare no conflict of interest.

Freely available online through the PNAS open access option.

Data deposition: The coordinates and structure factors have been deposited in the Protein Data Bank, www.pdb.org (PDB ID codes 3TXM and 3TXN).

¹To whom correspondence may be addressed. E-mail: bracher@biochem.mpg.de or baumeist@biochem.mpg.de.

This article contains supporting information online at www.pnas.org/lookup/suppl/doi:10.1073/pnas.1117648108/-DCSupplemental.

contact interfaces between Rpn6 and subunits of both the CP and RP.

Results and Discussion

Crystallization and Structure Solution. Rpn6 of *D. melanogaster* was expressed as a soluble 6xHis-tag fusion protein in *Rhodococcus erythropolis* (22). The 6xHis-tag was cleaved for biochemical analysis. Size-exclusion chromatography suggested that Rpn6 is monomeric in physiological buffer. Crystals from the 422-residue full-length protein showed only weak diffraction to approximately 9 Å resolution. To find a better construct for crystallization, we performed a limited proteolysis experiment using Proteinase-K. Mass spectrometry analysis of the most prominent SDS-PAGE fragment bands showed that the N-terminal region up to residue 29 is most sensitive to protease cleavage, indicating that it is flexibly linked. At higher protease concentrations, the protein is furthermore nicked at position 337, which maps to the PCI module (Fig. 1A). The Rpn6 construct comprising residues 30–422 yielded hexagonal crystals diffracting to 2.5 Å resolution. The crystal structure was solved by Gd-MAD at 3.0 Å resolution (Table S1). The model comprises residues 38–390 (Fig. 1B); the remaining residues were not resolved in the electron density and are presumably disordered.

Structure Overview. The crystal structure of Rpn6 consists of an α -helical solenoid followed by the PCI module (Fig. 1B). The overall shape is that of a right-handed suprahelical turn with approximate dimensions of 100 Å \times 45 Å (height \times width). The solenoid contains a slightly elongated N-terminal capping helix and five double-helix repeats with structural similarity to tetratricopeptide repeats (TPR). However, the helices are approximately one turn longer than in canonical TPR units; i.e., each repeat contains approximately 40 residues compared to 34 for TPRs. A conserved sequence signature for the Rpn6 repeats

could not be detected. The hydrophobic final helix of the solenoid, α 11, forms the central hub of a helix bundle, contacting helices α 12, α 14, and α 16 of the PCI module (Fig. 1C). This interaction enables additional contacts between α 9 and α 16 that reinforce the solenoid-PCI module interface, strongly suggesting that the orientation of the two domains is rigidly fixed to form the right-handed suprahelical configuration. Thus, there is no discrete N-terminal boundary of the PCI module, which supports the conclusion of prior bioinformatic analyses of PCI-protein sequences (14). The winged-helix subdomain of Rpn6 has an elongated first helix, α 16, which is markedly kinked in the center. Its N-terminal segment forms part of the helix bundle (Fig. 1C). The three-stranded antiparallel β -sheet of the PCI module is located at the tip of the suprahelical structure. α 18, the so-called recognition helix in canonical winged-helix transcription factors, is arranged perpendicular to the long axis of the protein. In DNA complex structures, this helix is placed into the major groove of DNA (23). Whether the corresponding structure in Rpn6 serves such a function is unknown, but might be worth further investigation. The 26S proteasome has been implicated to play a role in transcription (24) and DNA double-strand repair (25), which could require physical association of the 26S proteasome to nucleic acid. Comparison with the other known structures of PCI module proteins, Csn7 and eIF3 κ (13, 15), indicated that the winged-helix subdomains are less divergent than the N-terminal helix bundles (Fig. S1). The elongated helices in the Rpn6 helix bundle (helices α 12, α 14, α 16) appear to ensure a rigid connection to the α -solenoid; these elongations are absent in Csn7 and eIF3 κ . In addition, the proximal part of the helical bundle subdomain in all three structures appears to function as a buttress for the winged-helix domain.

Rpn6 Surface Conservation. To identify functionally important regions, we performed an extensive sequence alignment of 21 putative Rpn6 sequences (Fig. S2) and mapped the similarity score onto the surface of the crystal structure (Fig. 2A). In the solenoid segment, a large continuous area of increased surface conservation was found on the convex outer face between helix α 8 and α 10 (region I, Fig. 2A). This area has few surface charges (Fig. S3B). The adjacent loop connection between helices α 6 and α 7 (residues 158–162) is also highly conserved. On the concave face, the adjacent residues Lys82, Lys84, Lys87, Arg90, and Phe124 are almost invariant. All these areas face approximately in the same direction, while there is essentially no surface conservation on the opposite (convex) side (Fig. 2A), strongly suggesting that the former is involved in contacts with other subunits of the 26S proteasome complex, while the latter is exposed to solvent.

Surface conservation in the PCI module of Rpn6 is limited to two smaller areas located at the flanks on the β -sheet (regions II and III, Fig. 2B). Region II includes the end of helix α 16, strand β A and the connecting linker. Region III is composed of helix α 18 and strand β B. Both are predominantly hydrophobic, implying that they might serve as protein–protein interfaces (Fig. S3). Interestingly, region II and region III of adjacent Rpn6 chains contact each other in the crystal lattice. The alignment of the β -sheets creates a continuous β -ribbon that traverses the crystals along the 6-fold screw axis (Fig. S4A), suggesting that the six PCI subunits in the lid might be arranged similarly within the complex. The buried surface area of approximately 460 Å² on each partner is probably too small for a stable interaction consistent with our finding that Rpn6 is monomeric in solution. This observation suggests that other interactions must contribute to complex formation. A likely candidate for this additional interface is a conserved region at the C-terminus (residues 396–419) that was disordered in the crystal structure. In agreement, the sequence alignment suggests that this segment is flexibly attached to the PCI module via a poorly conserved linker (Fig. S2). Secondary structure prediction strongly suggests that the respective

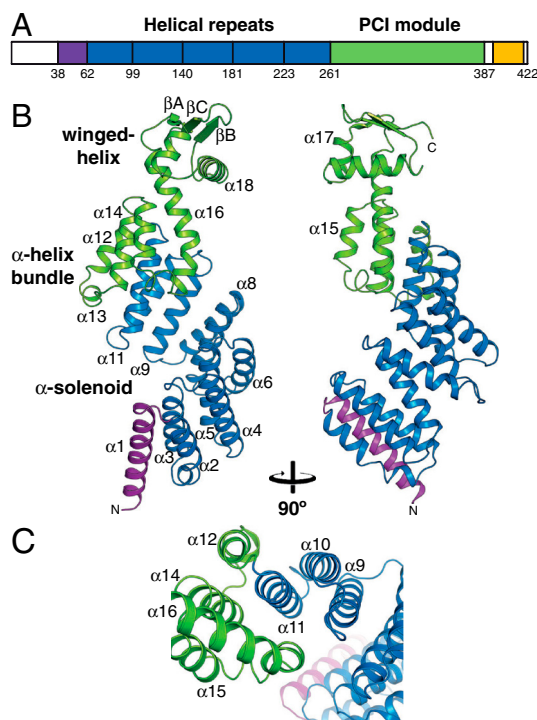


Fig. 1. Crystal structure of Rpn6. (A) Domain structure of Rpn6. The purple region denotes a capping helix; the yellow region is predicted to be α -helical. (B) Ribbon representation of Rpn6, colored by domain structure. Two views related by 90° rotation are shown. N and C termini and selected secondary structure elements are indicated. (C) Detailed view of the interface between the solenoid fold and the PCI module.

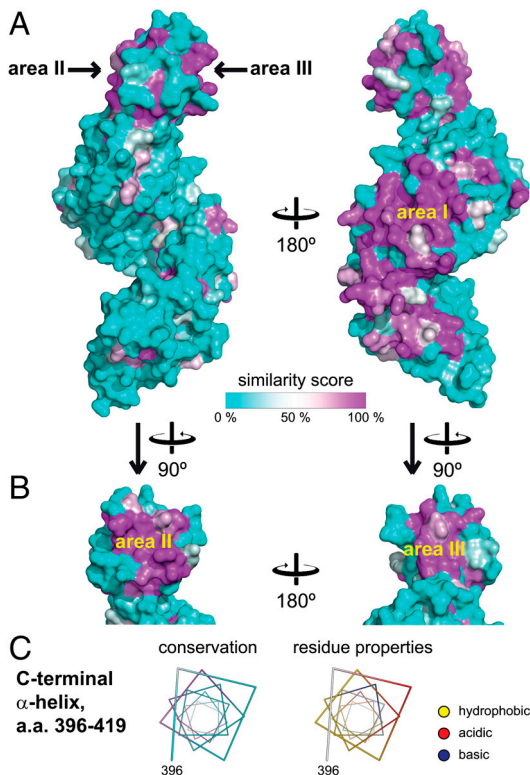


Fig. 2. Surface analysis of Rpn6. (A) Surface conservation mapped onto the surface of Rpn6. On the left, the same orientation as in Fig. 1A is shown. The similarity score from a multiple alignment of 21 related sequences (Fig. S2) was mapped onto the molecular surface of Rpn6. A cyan-white-magenta color gradient indicates increasing surface conservation. Regions I, II, and III are indicated. (B) Side views on the winged-helix subdomain. (C) The predicted C-terminal helix. The helix is represented as a helical wheel, and residue properties are indicated. (Left) Conservation is represented using the same color scheme as in panel A. (Right) Hydrophobic side chains are indicated in yellow. Positively and negatively charged functional groups are colored blue and red, respectively. The rest of the surface is shown in white.

region forms an amphipathic α -helix (4). Mapping conservation and surface properties on this predicted helix shows that conservation is limited to the hydrophobic face (Fig. 2C), suggesting that it is involved in interactions with other subunits, probably in a coiled-coil conformation. Intriguingly, all proteasomal PCI subunits were predicted to comprise such a helical segment C-terminal to the PCI module (4).

Interactions of Rpn6 Within the Lid. To test whether or not the PCI subunits interact with each other in the lid subcomplex, we incubated Rpn6 separately with 6xHis-tagged Rpn5, Rpn7, or Rpn9 of *D. melanogaster*, followed by Ni-affinity precipitation (Fig. 3A). Under the conditions tested, only Rpn6 and Rpn7 formed a stable binary complex. To analyze this interaction in more detail, mutations were introduced into Rpn6 (Fig. 3B). At the center of region I, we replaced the highly conserved peptide sequence 230-SYFYE-234 with KAFYK, yielding mutant M1 (Fig. 3C). Similarly, Rpn6 mutants M2 and M3 were generated by analogous substitutions of conserved peptide motifs in regions II and III, respectively. Finally, we removed the putative C-terminal α -helix by truncation at position 391 (M4). Interaction analysis of these mutant Rpn6 forms with 6xHis-tagged Rpn7 clearly showed that both an intact region III and the putative C-terminal helix are required for the interaction (Fig. 3D). This finding strongly suggests that the observed interaction is specific. Rpn6 and Rpn7 are thus likely to be in direct contact with each other in the lid, probably employing a bipartite interface.

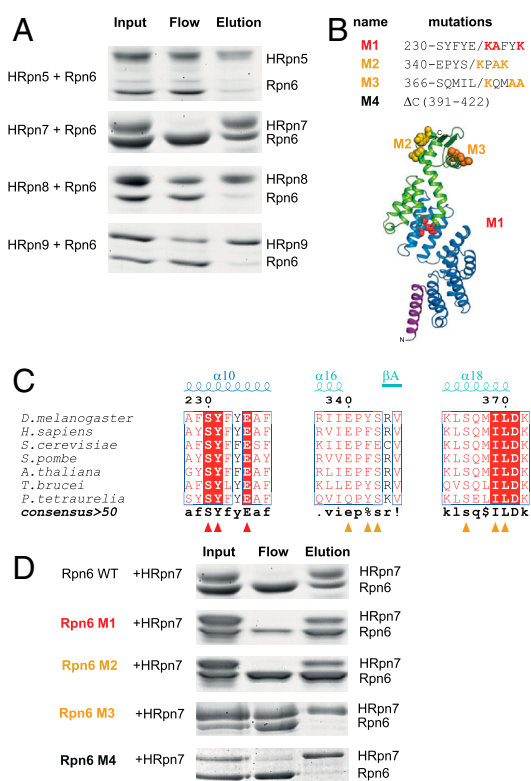


Fig. 3. Binary interaction of Rpn6 and Rpn7. (A) Probing for direct interactions of Rpn6 with lid particle subunits. Purified Rpn6 was incubated individually with His-tagged Rpn5, Rpn7, Rpn8, or Rpn9 from *D. melanogaster*. The Coomassie-stained SDS-PAGE gels show the initial mixtures, unbound proteins, and proteins precipitated with Ni-affinity resin. (B) Location of Rpn6 mutations in the structure. The respective amino acid residue substitutions are indicated. Mutated residues are shown in space-filling mode. (C) Excerpts from Rpn6 sequence alignment showing the mutated regions. (D) Both the PCI module interface region III and the C-terminal helix of Rpn6 are required for the interaction with Rpn7. His-tagged Rpn7 was incubated with either wild-type Rpn6(30-422) or Rpn6(30-422) mutants M1, M2, M3, or M4 and analyzed as described for panel A.

Location of Rpn6 in the 26S Proteasome. Finally, we fitted the crystal structure of Rpn6 into the 9.1 Å cryo-EM density of the 26S proteasome from *S. pombe*, which is the highest-resolution map available so far (10) (Fig. 4A). An exhaustive six-dimensional real-space search yielded a single solution, with high confidence (Fig. S5). The size of Rpn6 (49 kDa), its distinctive shape, and the prevalence of α -helices enabled the high-precision fit into the map (Fig. S6). We estimate that the accuracy of the fit considerably exceeds the resolution of the map (9 Å), probably by an order of magnitude. In the resulting model, Rpn6 forms a protrusion that is located at the outer rim of the lid particle, reaching down to the ATPase and alpha rings with its α -solenoid segment (Fig. 4A). This interface appears to be the most extensive direct contact between the lid and core particles (a second contact formed by a protrusion to the left of Rpn6 appears weaker). There is additional density at the N-terminus of the Rpn6 model that might correspond to residues 1-37, most of which were not included in the crystallization construct. For Rpn6 of *S. pombe*, an additional pair of helices was predicted for this segment and included in our homology model (Fig. 4B). Regions on Rpn6 with high surface conservation match almost perfectly with the areas buried in the complex, while the rather poorly conserved face projects toward the solvent (compare Figs. 2A and 4A).

The subunits contacted by the solenoid domain of Rpn6 were previously assigned as Rpt6 and Pre8 (alpha2) using the 9.1 Å cryo-EM density of the 26S proteasome from *S. pombe* and

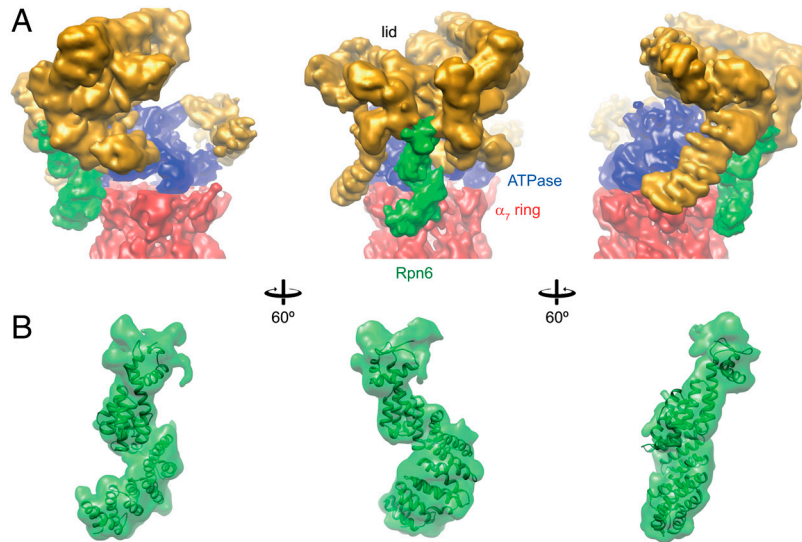


Fig. 4. Location of Rpn6 in the 26S proteasome. (A) Rpn6 density within the 9 Å cryo-EM density of the 26S proteasome from *S. pombe*. Three views are shown. The lid, base, and core subcomplex densities are indicated in gold, blue, and red, respectively. Density ascribed to Rpn6 is colored green. The core particle is clipped off at the β_7 ring. (B) Detailed view of the Rpn6 fitted into the EM envelope. Density assigned for Rpn6 was segmented from the map. The homology model of Rpn6 from *S. pombe* including the predicted N-terminal helices $\alpha(-1)$ and $\alpha 0$ are included. Similar orientations as in panel A are shown.

cross-linking data (10). For both, high-confidence molecular models are available (7, 26–28). Both subunits share a conspicuous surface conservation in the Rpn6 contact areas, which is indicative of coevolution of the interface residues (Fig. 5 A–E). Interestingly, conditional mutation of Rpt6 in *S. cerevisiae* resulted in the same G2/M phase transition arrest as the Rpn6 deletion (20, 29). Closer inspection reveals that the CP subunit Pre8 is in proximity to the N-terminus of $\alpha 3$ (residues 79–85), the loop between $\alpha 4$ and $\alpha 5$ (118–122), and the loop between $\alpha 6$ and $\alpha 7$ (157–160) (Fig. 5 B and C). Together, these elements form an extensive, conserved interface. Under the reasonable assumption that the peptide backbones in the complex are similar to those in the individual crystal structures, a tentative assignment of molecular interactions is possible: The small side chains of Ser79^{Rpn6} and Ala81^{Rpn6} (*S. pombe* numbering, add 2 for *D. melanogaster*) enable tight contacts to $\alpha 7$ of Pre8. The adjacent residues Lys80^{Rpn6}, Lys82^{Rpn6}, and Lys85^{Rpn6} are in hydrogen-bonding distance to Glu183^{Pre8}/Asp185^{Pre8}, Asp240^{Pre8}, and Asp243^{Pre8}, respectively. Because of the proximity to Asp159^{Rpn6} and Asp160^{Rpn6}, the C-terminal Val245^{Pre8} might rearrange to form a salt bridge with its carboxylate group to Arg88^{Rpn6}. The Val245^{Pre8} side chain would then point into a hydrophobic pocket formed by Phe122^{Rpn6}, Ala126^{Rpn6}, and Arg88^{Rpn6}. In an alternative scenario, the side chains of Phe122^{Rpn6} and Met158^{Rpn6} might rearrange locally and engage in contacts with two hydrophobic pockets located between helices $\alpha 7$ and $\alpha 6$, and at the loop connection between $\alpha 5$ and $\alpha 6$ of Pre8, respectively. Moreover, Asp159^{Rpn6} is in hydrogen-bonding distance to Arg177^{Pre8} and His189^{Pre8}; Lys119^{Rpn6} may form a salt bridge with Glu183^{Pre8}. The exposed side chain of residue Tyr199^{Rpn6}, which is located in the strongly conserved loop between helices $\alpha 8$ and $\alpha 9$ (residues 186–202), could reach toward the highly conserved Lys196^{Pre8}.

The Rpt6–Rpn6 interface involves Rpn6 helices $\alpha 8$ and $\alpha 10$ (Fig. 2, area I), which are located opposite to Rpt6 helices $\alpha 12$ and $\alpha 13$ (i.e. helices 3 and 4 in its four-helical bundle subdomain) (Fig. 5 D and E). Specifically, the conserved helix $\alpha 8$ of Rpn6 aligns with helix $\alpha 12$ in Rpt6. Residues Thr234^{Rpn6}, Ser227^{Rpn6}, Tyr228^{Rpn6}, and Glu231^{Rpn6} (the latter three mutated in Rpn6-M1, Fig. 3) at the groove between helices $\alpha 8$ and $\alpha 10$ of Rpn6 cradle the highly conserved C terminus of Rpt6 helix $\alpha 12$, extending the contact area. While Tyr228^{Rpn6} is placed for con-

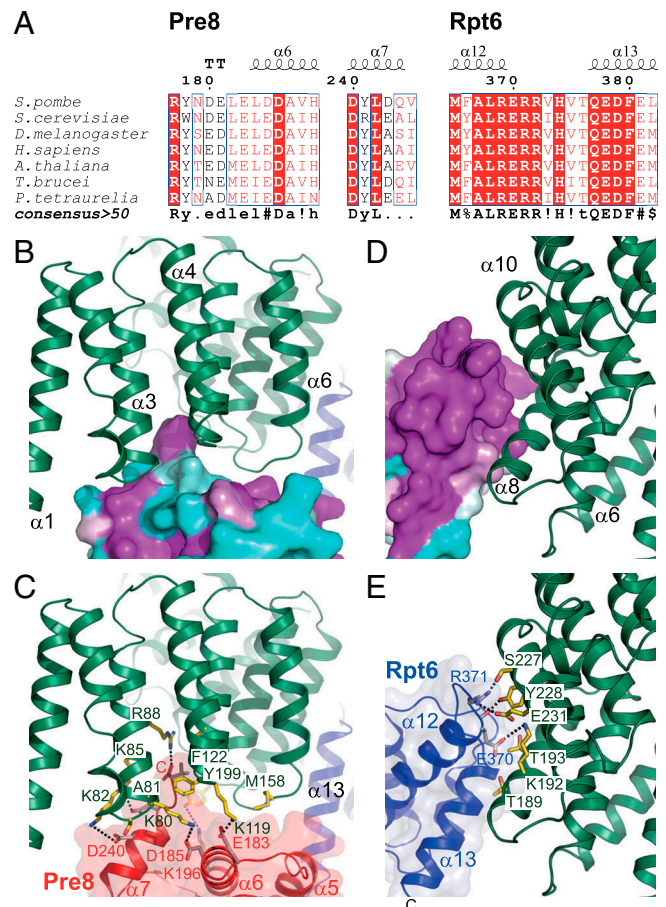


Fig. 5. Putative interactions of Rpn6 with Pre8 and Rpt6. (A) Excerpts from Pre8 and Rpt6 sequence alignments for the Rpn6 contact regions. (B and C) Detailed view of the interactions with Pre8. (Upper) The similarity score of an extensive alignment of Pre8 sequences mapped onto the homology model surface. Rpn6 is shown as a green ribbon. (Lower) Putative key interactions at the interface. Both proteins are shown in ribbon representation. Selected side chains are shown as sticks. Putative hydrogen bonds are indicated by dashed lines. (D and E) Detailed view of the interactions with Rpt6.

tacting the backbone at Rpt6 residue 370, the Arg371^{Rpt6} side chain is in hydrogen-bonding distance to both Ser227^{Rpn6} and Glu231^{Rpn6}. Glu370^{Rpt6} could form hydrogen bonds with Lys192^{Rpn6} and Asn196^{Rpn6}.

Interestingly, surface conservation on Rpn6 extends toward the lid beyond the observed contact area—for example, Ala186^{Rpn6} is extending the conserved edge of helix $\alpha 8$ continuing from Thr189^{Rpn6} and Thr193^{Rpn6}. This conservation suggests that Rpn6 could accommodate different conformational states of the ATPase ring. “Wobbling” or “wagging” motions of the active ATPase ring relative to the CP have been proposed (30, 31), and ATP-dependent structural changes involve binding of ubiquitin conjugates (32). In addition, there is structural evidence for a wagging motion of the whole RP (30).

The tip of the PCI module of Rpn6 is part of a horseshoe structure with six radially projecting protrusions that are included in the lid density (Fig. 4A). The contact points within the horseshoe coincide with the conserved regions II and III at the flanks of the β -sheet in Rpn6 (Fig. 4B). Region III, which was implicated in direct interactions of Rpn6 with Rpn7 (Fig. 3D), is situated to the right (Fig. 4B), suggesting that this density corresponds to Rpn7. Furthermore, yeast-two hybrid assays indicate a physical interaction of Rpn6 and Rpn5 via their PCI modules (21), suggesting that the density to the left of Rpn6 represents Rpn5. It is thus tempting to speculate that the horseshoe represents the density for the six proteasome PCI subunits, arranged like the Rpn6 chains in the crystal (Fig. S4A). According to this hypothesis, the interacting winged-helix subdomains form the inner rim, and the N-terminally adjacent α -helical bundles and solenoids form the protrusions. At the current resolution, the density for the C-terminal helix of Rpn6 cannot be assigned with confidence.

Arrangement of the PCI Subunits in the RP. Our mutational analysis showed that the winged-helix subdomain in the PCI module of Rpn6 is important for interactions with the PCI subunit Rpn7, consistent with the proposed function as a PCI:PCI interaction module (14). In addition to an intact winged-helix motif, the conserved C-terminal helix of Rpn6 is required for the interaction with Rpn7. This requirement for an additional contact might explain why we were not able to identify a second PCI binding partner of Rpn6. Rpn5, Rpn6, and Rpn9 form a subcomplex together with Rpn8 and Rpn11 (33), suggesting that one of the latter non-PCI subunits is required for the attachment of Rpn6 to Rpn5 in addition to the subunit II–III interface. The assembly pathway of the lid suggests that the PCI subunits Rpn3 and Rpn7 form a dimer, and PCI subunit Rpn12 attaches to the Rpn3/Rpn7 dimer after its binding to the Rpn6/Rpn5/Rpn8/Rpn9/Rpn11 pentamer (33). Thus, Rpn6 and Rpn7 followed by Rpn3 and Rpn12 could form the right end of the horseshoe, perhaps stabilized by coiled-coil interactions of their C-terminal helices; the interaction of Rpn6 with Rpn5 would require Rpn8 and Rpn11, resulting in the second subcomplex. The sequence of PCI subunits in the horseshoe structure would thus be (from the left) Rpn9–Rpn5–Rpn6–Rpn7–Rpn3–Rpn12 (Fig. S4B). Such a model is consistent with native MS analysis of the COP9/signalosome, in which each subunit of the lid subcomplex has a homolog (34).

Thus, the lid and COP9/signalosome architectures might be evolutionarily conserved.

Conclusions

In our hybrid structure, Rpn6 contacts at least four subunits from three functional units of the proteasome, the lid, the ATPase, and the proteolytic core particle. Interactions with Rpn6 thus appear to reinforce the contacts between the lid and base and also between the regulatory and core particles. This Rpn6 role is consistent with increased occurrence of partially assembled proteasome particles in the temperature-sensitive *rpn6-2* mutant of budding yeast (21). Interestingly, this mutant harbors mutations both at the interface to the alpha ring, F132L (residue F122 in *S. pombe*) and the lid subunits Rpn5 and Rpn7, L377P (residue L365 in *D. melanogaster*). The latter mutation would presumably interrupt helix $\alpha 18$, compromising the structural integrity of the winged-helix subdomain.

Because of the symmetry mismatch between the heptameric alpha ring and the hexameric AAA-ATPase, their contacts appear rather sparse and weak, thus enabling relative motions. Indeed, symmetry mismatches have often evolved to allow for motions of macromolecules during their functional cycle (35). Thus, Rpn6 appears to have a pivotal role in holding the complex together by acting as an additional clamp between RP and CP. Monomeric Rpn6 might also be functionally important. The reported interactions of Rpn6 with the ubiquitin ligase regulatory complex COP9/signalosome probably control its own degradation (19, 36), which might in turn regulate the assembly and activation of 26S proteasomes through the availability of monomeric Rpn6. Such a regulation is consistent with the critical role of Rpn6 for the integrity of the 26S proteasomes complex.

Materials and Methods

Detailed experimental procedures are given in *SI Materials and Methods*. Briefly, Rpn6 from *D. melanogaster* was expressed as a His₆-tag fusion protein including a tobacco etch virus (TEV) protease site in *R. erythropolis* (L-88) cells and purified by Ni²⁺-immobilized metal affinity chromatography, TEV cleavage, Mono-Q anion exchange chromatography, and Superose-12 size-exclusion chromatography. Crystals were grown using 100 mM Tris-HCl pH 7.5 200 mM Li₂SO₄ and 12% PEG-3350 as a precipitant. The Rpn6 crystal structure was solved by multiwavelength anomalous dispersion using gadolinium(3+), using diffraction data acquired at the European Synchrotron Radiation Facility (ESRF), Grenoble, France. The exact position and orientation of Rpn6 in the 9.1 Å electron density map of the 26S proteasome was determined by an exhaustive six-dimensional search procedure.

ACKNOWLEDGMENTS. We thank the staff of the Joint Structural Biology Group at the European Synchrotron Radiation Facility, Grenoble, France, of the Max-Planck-Institute of Biochemistry Crystallization Facility and the Max-Planck-Institute of Biochemistry Core Facility for their excellent support; and Johannes Söding for valuable discussions. Materials for the *R. erythropolis* expression system were kindly provided by Khalid Ibrahim Sallam and Noriko Tamura, Sapporo, Japan. This work was supported in part by funding from the European Union 7th Framework Program PROSPECTS (Proteomics Specification in Space and Time Grant HEALTH-F4-2008-201648). F.F. is grateful to a Career Development Award from the Human Frontier Science Project. K.L. was supported by continuous mentorship from Prof. Haim J. Wolfson as well as a fellowship from the Clore Foundation Ph.D. Scholars program.

- Buchberger A, Bukau B, Sommer T (2010) Protein quality control in the cytosol and the endoplasmic reticulum: Brothers in arms. *Mol Cell* 40:238–252.
- Glickman MH, Ciechanover A (2002) The ubiquitin-proteasome proteolytic pathway: Destruction for the sake of construction. *Physiol Rev* 82:373–428.
- Hershko A, Ciechanover A, Varshavsky A (2000) Basic Medical Research Award. The ubiquitin system. *Nat Med* 6:1073–1081.
- Förster F, Lasker K, Nickell S, Sali A, Baumeister W (2010) Toward an integrated structural model of the 26S proteasome. *Mol Cell Proteomics* 9:1666–1677.
- Tanaka K (2009) The proteasome: Overview of structure and functions. *Proc Jpn Acad Ser B Phys Biol Sci* 85:12–36.
- Voges D, Zwickl P, Baumeister W (1999) The 26S proteasome: A molecular machine designed for controlled proteolysis. *Annu Rev Biochem* 68:1015–1068.
- Groll M, et al. (1997) Structure of 20S proteasome from yeast at 2.4 Å resolution. *Nature* 386:463–471.
- Löwe J, et al. (1995) Crystal structure of the 20S proteasome from the archaeon *T. acidophilum* at 3.4 Å resolution. *Science* 268:533–539.
- Unno M, et al. (2002) The structure of the mammalian 20S proteasome at 2.75 Å resolution. *Structure* 10:609–618.
- Bohn S, et al. (2010) Structure of the 26S proteasome from *Schizosaccharomyces pombe* at subnanometer resolution. *Proc Natl Acad Sci USA* 107:20992–20997.
- Glickman MH, et al. (1998) A subcomplex of the proteasome regulatory particle required for ubiquitin-conjugate degradation and related to the COP9-signalosome and eIF3. *Cell* 94:615–623.
- Kim T, Hofmann K, von Arnim AG, Chamovitz DA (2001) PCI complexes: Pretty complex interactions in diverse signaling pathways. *Trends Plant Sci* 6:379–386.
- Dessau M, et al. (2008) The Arabidopsis COP9 signalosome subunit 7 is a model PCI domain protein with subdomains involved in COP9 signalosome assembly. *Plant Cell* 20:2815–2834.

Supporting Information

Pathare et al. 10.1073/pnas.1117648108

SI Materials and Methods

Cloning and Purification of Rpn6. Rpn6 from *Drosophila melanogaster* was cloned as N-terminal 6xHis-tag fusion protein into a modified pTipRC1 plasmid with a tobacco etch virus (TEV) protease cleavage site in between 6xHis-tag and the *rpn6* gene. Protein expression was carried out in *Rhodococcus erythropolis* (L-88) (1), where the resulting strain was grown at 30 °C in 5 L of LB medium. Protein production was induced with 0.5 $\mu\text{g mL}^{-1}$ thioestrepton for another 24 to 48 h. Cells were sedimented at 4,000 g and washed with sterile water. The pellet (20 g) was resuspended in 50 mL lysis buffer (50 mM sodium phosphate pH 8.0, 10 mM imidazole, 300 mM NaCl). Complete protease inhibitor cocktail (Roche Biotech) and 1 mg mL^{-1} lysozyme were added, and the mixture incubated for 2 h on ice. Subsequently, 100 ppm Benzonase was added, followed by ultrasonication on ice. Cell debris was removed by ultracentrifugation at 28,000 \times g. His-tagged Rpn6 was purified by affinity chromatography using Ni-NTA beads (GE Healthcare) according to the supplier recommendations. Fractions containing Rpn6 were pooled, augmented with TEV protease for removal of the 6xHis-tag, and incubated for 12 h at 4 °C in a dialysis chamber equilibrating against 25 mM Tris HCl pH 7.5. TEV protease was removed by MonoQ anion exchange chromatography, using a linear salt gradient to 1 M NaCl in 25 mM Tris HCl pH 7.5. Size-exclusion chromatography (SEC), using Superose-12 (GE Healthcare) equilibrated with 20 mM Hepes NaOH pH 7.5, 300 mM NaCl, and 1 mM DTT was used as final purification step.

Limited proteolysis. Full-length Rpn6 at 0.5 mg mL^{-1} was subjected to limited proteolysis, using increasing concentrations of Proteinase-K (0.025–0.1 mg mL^{-1}). After 30 min incubation at 20 °C, samples were analyzed by SDS-PAGE followed by in-gel digestion and peptide mass spectrometry. Samples with prominent digestion products were subjected to liquid chromatography–mass spectrometry analysis to measure apparent molecular masses to be able to determine actual proteolytic sites.

Crystallization. Crystals of Rpn6(30–422) were grown by the sitting drop vapor diffusion method at 4 °C and 18 °C, mixing equal volumes of Rpn6(30–422) (25 mg mL^{-1} in 20 mM Hepes NaOH pH 7.5, 300 mM NaCl, and 1 mM DTT) with a precipitant containing 100 mM Tris HCl pH 7.5 200 mM Li_2SO_4 , 12% PEG-3350. For cryoprotection, crystals were transferred stepwise into 100 mM Tris HCl pH 7.5, 300 mM Li_2SO_4 , 15% PEG-3350 and 20% glycerol before being flash-frozen in liquid nitrogen.

Structure Determination. Diffraction data were collected at the European Synchrotron Radiation Facility (ESRF) in Grenoble, France. The data were processed with XDS (2) and transferred into the CCP4 format using Pointless (3), Scala (4), and Truncate (5). The structure was solved using crystals soaked with 0.5 mM GdCl_3 . Four Gd sites were found in a MAD dataset using SHLXD (6) as implemented in HKL2MAP (7). This solution was further refined with Sharp (8). Density modification was subsequently carried out using Resolve (9). A preliminary model was manually built in the resulting map using Coot (10). For final model building and refinement, nearly isomorphous native data

were used. Iterative cycles of manual model building and refinement with Refmac (11), as implemented in the CCP4 interface (12), were carried out. The final model contains Rpn6 residues 38 to 390, two sulphate, two glycerol, and 49 water molecules. Nonglycine residues facing solvent channels without discernable side-chain density were modeled as alanines.

Site-Directed Mutagenesis. Site-directed mutations in Rpn6 were introduced with the QuikChange site-directed mutagenesis kit (Stratagene) using pTipRC-Rpn6 as the template.

Coprecipitation Assay. Different subunits from the *D. melanogaster* regulatory particle were used for the coprecipitation assay. Binary interactions of these subunits were studied by mixing Rpn6 with other subunits having a 6xHis-tag. Proteins were mixed at 1:1 molar ratio and incubated with Ni-NTA Superflow beads at 20 °C for 45 min. The mixtures were applied to spin column bodies (Qiagen), washed with the washing buffer, and the retained proteins were eluted with the elution buffer. The fractions were analyzed by SDS-PAGE.

EM Density Fitting. The exact position and orientation of Rpn6 in the electron density map of the 26S proteasome was determined by an exhaustive six-dimensional search procedure. The atomic coordinates of Rpn6 were converted into a gray-scale volume by assigning the sums of atomic numbers for all atoms contained in the corresponding voxels. This Rpn6 density volume was low-pass filtered to a resolution of 6.4 Å and used as a template for a cross-correlation based search by screening three translational and three rotational parameters. The rotational search was performed with an angular increment of 2° using MOLMATCH (13). The position of the maximal normalized cross-correlation coefficient ($CCC_{\text{max}} = 0.48$) and the corresponding rotational parameters were determined, and the original atomic coordinates of Rpn6 were transformed accordingly (see also Fig. S5). In addition, we computed a Z-score for the orientation-specificity for each of the determined positions as described previously (14).

Bioinformatics Methods. A Dali search (15) of the Protein Data Bank (PDB) using the solenoid part of Rpn6 revealed several prokaryotic proteins with structurally similar repeats but disparate biological functions: DrR162B (PDB ID code 3GW4), PlcR [PDB ID code 2QFC (16)], and MalT [PDB ID code 1HZ4 (17)].

HHpred (18) was used for identification of structural templates and their alignment to the target sequence of *Schizosaccharomyces pombe* Rpn6. Our *D. melanogaster* Rpn6 crystal structure covered residues 38 to 387, and TOM70 (PDB ID code 2GW1) was used as an additional template for residues 4 to 100. The C-terminal residues 388–421 were not modeled. Comparative models were built using MODELLER (19) and further refined in the context of the EM map using MDFF (20).

Structural figures were prepared using PyMOL (<http://www.pymol.org>) and Chimera (<http://www.cgl.ucsf.edu/chimera/>). Alignment figures were created with ESPript (21).

1. Nakashima N, Tamura T (2004) A novel system for expressing recombinant proteins over a wide temperature range from 4 to 35 degrees C. *Biotechnol Bioeng* 86:136–148.
2. Kabsch W (2010) XDS. *Acta Crystallogr D Biol Crystallogr* 66:125–132.
3. Evans P (2006) Scaling and assessment of data quality. *Acta Crystallogr D Biol Crystallogr* 62:72–82.

4. Evans PR (1997) Scala. *Joint CCP4 + ESF-EACBM Newsletter on Prot Crystallogr* 33:22–24.
5. French G, Wilson K (1978) On the treatment of negative intensity observations. *Acta Crystallogr A* 34:517–525.


```

                                1      10      20      30      40
D.melanogaster  . . . . .MAGATLFERAQALSSVNREEQDSSLLNKLVLRDQEG. . . . .AEENDE
H.sapiens      . . . . .MAAAAVVEFQRAQSLSTDRASIDILHSIVKRDIO. . . . .ENDE
O.dioica      . . . . .MAGAACVAQPT. . . . .NNDLQQLYHDLMSAKE. . . . .RSDQ
C.albicans     SIHHLQPLQNMSSGQLLEEARAKAVTNKQYDEAEIKYKQIINPSESSTSTTTTTTTTFTA
S.cerevisiae   . . . . .MSLPGS.KLEEARRLVNEKQYNEAEQVYLSLID. . . . .KDSSQSSAAAGASVDD
Y.lipolytica  . . . . .MTLEETLASAKTAGDKGNLVEAEKLYREILD. . . . .KQAGTNE
C.posadasii   . . . . .MAPNSETAALLKEATALS.KTDPSSKAEITFCQVLSLG. . . . .TGSFTE
P.brasiliensis . . . . .MAG.PDDASLLAEAKNLV.KTDPKAESEYQKILSKG. . . . .VGSFTE
T.stipitatus  . . . . .MAST.SASQRTBEAKSLA.SKDPKASEQIYRDRVSSG. . . . .VGKTE
N.crassa      . . . . .MAQG.EASERVREAQKVV.STDPRQAEQIYKDKITISKPP. . . . .SVTSD
T.melanosporum . . . . .MGRLEEAGEIQ.KRDPARAEAMYKEMISKP. . . . .PGMND
S.pombe       . . . . .MSSKSSLELANNVKSNDIEKAIKYKELVNLKG. . . . .VSKDE
D.discoideum  . . . . .MNNWKEQLEEIGNCO. . . . .DSNKATQDYNKILTIQ. . . . .E
A.thaliana    . . . . .MVSYRAT.TETISLALAEANSSEAITLYQVILE. . . . .DPSSSP
P.patens      . . . . .MLREVIY. . . . .HPASTA
C.rheinhardtii . . . . .MSAELETRLKSATELGATDVPGAAAQIKGLVILE. . . . .ESSNDA
N.gruberi     MTDNTTSDQQTFYTTLFEKATKEEEKQNTAEAIKIFTOVINGE. . . . .MSKKN
T.brucei      . . . . .MEKDLDSLWDTAEDFIADGRRTEARGVLEDIVSTD. . . . .VTADDA
C.elegans     . . . . .MSATPVTLKAVQSEVSAQT. . . . .AKSSE
P.tetraurelia . . . . .MATLIEKFOALLQEVNARLDTNNLEAALLKLLTFDSK. . . . .SE
T.vaginalis  .MDNEIPFVERLGINVDPKDFNVPLTQRAALLEDLIDEVLOGD. . . . .AHIE
consensus>50 . . . . .v. . . . .e

```

```

                                a1      a2      n1      a3
                                50      60      70      80      90      100
D.melanogaster  RIRIKKQGLLQGGELYKQEGKAKEADLLKVTTRPFLSSISKAKAAKLVRSVLDMLFLDMD
H.sapiens      EAVQVKEQSILELGSLLAKTQAAELGGLIKYVTRPFLNSISKAKAARLVRSLLDLFLDME
O.dioica      ETRKNEAKIIELGWELQKGNAKELEGVLKNVTRPFLGSSKAKAARLVRSVLDMLFLDMD
C.albicans     KQLQQQESAIIELGKIYETINEPTKSLDADSRSLGNFAKSKTAKIVKTLIEDFDKILIS
S.cerevisiae   KRRENEQESILELQGLYVTMGAKDKREFIPHSTIEMMGEFAKSKTKVVKLTLIEKFEOVP
Y.lipolytica  KSIQIQESAILINLGTLYASNKPKQDADLIHTSLTVMGFAKSKTAKIIRNLDLFAKVP
C.posadasii   AASRDYEAALVGLGELYRDKRPKELAEILRTSRSSFSFAKAKSAKLVRLDLPFAAIP
P.brasiliensis AASRDYEAALVGLGELYRDKRPKELAEILRTSRSSFSFAKAKSAKLVRLDLPFAAIP
T.stipitatus  SASRDYEAALVGLGELYRDKRKAHEADLIKSRDFAFSFAKAKTAKLVRLDLDLSEIP
N.crassa      AALREYEAALVGLGELYRDKPKSQGLVLDVTSRTVLSSFAKAKTAKLVRLDLDLFEAIP
T.melanosporum AALREYEAALVGLGELYRDARRTGEAEELIKASRSMSSFAKAKTAKIVRLDLDLFTTIP
S.pombe       KVANECQALTNISDLVVRNRRNDLAQLVQSPPLMANHSAKAKSAKIVRLDLDKFSGK
D.discoideum  SFDIIEKALIRLAKLFEVKGKGDQLETLIRSVRPFDFKSAKPKTKIVRNLIDPFSFIP
A.thaliana    EALIKKQATNLCDAITEKRGEDLRKLTKEPFSFLFAKAKTAKIVRNLIDPFAKIP
P.patens      EVLVYKQATLALDLSQEKKAELRGLITDRLRPYFNLFKAKTAKIVRNLIDPFAKIP
C.rheinhardtii EAVRIKQATISQLCELYIKANAQAADLITSLRGFNFAKAKTAKLVRSIIDSIAKVP
N.gruberi     VIKKKEAISLGIYATKGAQAAMELNKSRPFFQDLFAKAKTAKIVRLDLDLFTGK
T.brucei      IGLPAKRAIYRAELISVFKQTDMLVQLLSAIRSFFALPFAKAKTRVMRKMFDLNLNSG
C.elegans     AEVKRCEDLILSVSRQLAKFKDITGTRTLVESIRSFYDLVFKARASKLIRNDIVEHALTID
P.tetraurelia EHLKHKESAYNKLSSLYCKNKPQLVFCINKTHD.FSGHNQTRAAKIMRQIDVQSOVLE
T.vaginalis  ERVGFQVNHLELYVOANSEKFAFLLDHLAEYFTKLPKAKTAKLVRIIOLARKVP
consensus>50 . . . . .E. . . . .l. . . . .y. . . . .l. dl. . . . .r. . . . .kak.ak.vr.li# . . . . .

```

```

                                a4      a5      a6
                                110     120     130     140     150
D.melanogaster  A. . . . .GTEVQCKDCIEWAKQEKRTFQRQSLAHLIALLYFDTALVTEATLGAQ
H.sapiens      A. . . . .QVEVLCIECIEMAKSEKRTFRQALEARLVSLYFDTKRYQEAHLHLSGQ
O.dioica      S. . . . .AIGVEVDCKECIQWAMEEKRTYRQALEARLIMALLYFDTNKYKCLTLGQR
C.albicans     AKD. . . . .EKSIDIQIDVTKSSMQWAIESKLSFRQSLQLKLSDLLYQKHHKHAALINE
S.cerevisiae   D. . . . .SDDQIFVCEKSEIEFAKREKRVFKHSLSIKLAITLHYQKQVYKDSALIND
Y.lipolytica  S. . . . .DCDLOIAITOKCIEWAVSEKRNFRQSLQTRLVSLFLEKTYVYDALIND
C.posadasii   N. . . . .TDDIQISVIKSCIEWAVSERRSFRQNLLETFLVTIYMOKQSYDDALTLINS
P.brasiliensis N. . . . .TDDIQIIVIKSCIEWAVSERRSFRQNLLETFLVTIYMOKQSYDDALTLINS
T.stipitatus  N. . . . .TDDIQIIVIKSCIEWAVSERRSFRQNLLETFLVTIYMOKQSYDDALTLINS
N.crassa      D. . . . .SDDIQISVTKSCIEWATSERRSFRQNLLETFLVALYMAKQSYDDALTLING
T.melanosporum D. . . . .TDDIQISVTKSCIEWAIQERRSFRQNLLETFLVGLYLRHSYTEALTLINS
S.pombe       K. . . . .SFLQIEVANDCIKWAIKEKRTFRQALETRKLSLYDSSYTDALTLINT
D.discoideum  D. . . . .NLTLLIEVFKENIQWKDTRNRYRQRLTEKLFITLMEFAKDYANALSGLIT
A.thaliana    G. . . . .TDDLOITLCKEMVEVTRAEKRTFRQRVEARLALALMENKEYVEALALLST
P.patens      G. . . . .TDDLOISLQREMEVTRAEKRTFRQRVEARLALALMENKEYVEALALLST
C.rheinhardtii G. . . . .SLOVDVCKGQVEVATEKRTFRQRVIELRLASLYMQRDYPALALLITR
N.gruberi     G. . . . .SIAIQIEICRESIEWATEKRTFRQRVIESRLANLFLIKFEPESLEITR
T.brucei      A. . . . .SRQMEVCRDMIAWAQEKRTFRQRLQHRFAEVQFARNERQEAALTLQA
C.elegans     QGVGFALDHGKKEKIDLLNCGIWAATSNKREFRSLQARLIRLYNDIRDTNQAQKLAQD
P.tetraurelia G. . . . .TLEQVHCQFLTDCAKDKNFKHWQIRLALTYNEKFSQSGEITDK
T.vaginalis  G. . . . .TLEQADLCKKWITWAKDQERTFRQRIETEISELLEQHKWNEAELIQR
consensus>50 . . . . .qi. . . . .iewa. . . . .e.r.flrq.le.rL.l.q. . . . .y.eal.l.l.

```

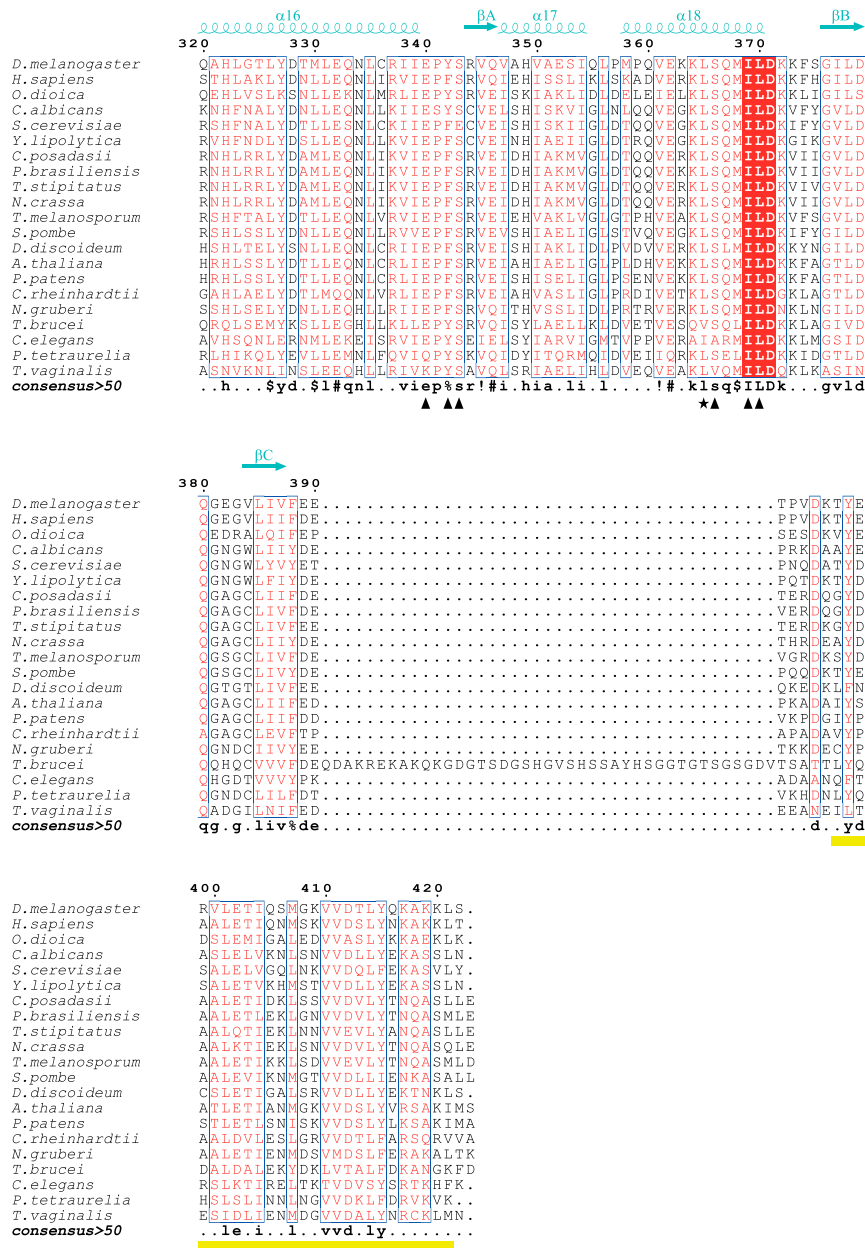



Fig. S2. Alignment of representative Rpn6 sequences. Amino acid sequences of selected Rpn6 homologs were aligned using Clustal-X. Secondary structure elements for the *D. melanogaster* Rpn6 are indicated above the sequences. The Rpn6 domain structure is indicated by purple, blue, and green coloring of secondary structure elements in the capping helix, α -solenoid, and PCI module, respectively. Similar residues are shown in red and identical residues in white on red background. Blue frames indicate homologous regions. The consensus sequence is shown at the bottom. The mutation sites, F132L and L377P, in *Saccharomyces cerevisiae* strain *rpn6-2* are indicated by asterisks. The mutations sites for *D. melanogaster* mutants M1, M2, and M3 are indicated by triangles. The position of the predicted C-terminal helix is indicated by a yellow bar below the alignment. The Uniprot accession codes for the sequences are: Q7KLV9, *Drosophila melanogaster*; O00231, *Homo sapiens*; E4XC34, *Oikopleura dioica*; Q59TN7, *Candida albicans*; Q12377, *Sacharomyces cerevisiae*; Q6C9R4, *Yarrowia lipolytica*; C5P9Z7, *Coccidioides posadasii* (strain C735); C1GHW5, *Paracoccidioides brasiliensis* (strain Pb18); B8M6N4, *Talaromyces stipitatus* (strain ATCC 10500/ CB5 375.48/QM 6759/NRRL 1006); Q96U28, *Neurospora crassa*; D5G146, *Tuber melanosporum* (strain Mel28); Q9P7S2, *Schizosaccharomyces pombe*; Q54UB5, *Dictyostelium discoideum*; Q9LP45, *Arabidopsis thaliana*; A9RB85, *Physcomitrella patens* subsp. patens; A81274, *Chlamydomonas reinhardtii*; D2UZW5, *Nae-gleria gruberi*; Q586L6, *Trypanosoma brucei*; P34481, *Caenorhabditis elegans*; A0BT65, *Paramecium tetraurelia*; A2DYJ9, *Trichomonas vaginalis*.

Table S1. Data collection and refinement statistics

Dataset	MAD			Native
	ESRF, ID23-1 <i>peak</i>	<i>inflection</i>	<i>remote</i>	
Beamline				ESRF, ID29
Wavelength, Å	1.71024	1.71072	1.03320	1.00686
Space group	$P6_1$			$P6_1$
Cell dimensions, a, b, c; Å	161.25, 161.25, 42.08;			161.30, 161.30, 42.10;
$\alpha, \beta, \gamma, ^\circ$	90, 90, 120			90, 90, 120
Resolution limits, Å*	40.42–3.4 (3.58–3.4)	40.47–3.4 (3.58–3.4)	38.89–3.0 (3.16–3.0)	52.78–2.5(2.65–2.5)
R_{merge}^*	0.063 (0.335)	0.054 (0.352)	0.048 (0.489)	0.046 (0.303)
I/σ^*	20.1 (5.2)	13.5 (2.9)	14.5 (1.9)	14.4 (2.6)
Multiplicity [†]	7.3 (7.6)	3.6 (3.7)	3.6 (3.7)	3.3 (3.3)
Completeness, %*	97.9 (98.5)	97.4 (97.7)	97.9 (96.6)	99.3 (99.0)
Phasing				
Sites	4 Gd			—
Phasing power ano	2.172	1.405	0.447	—
Phasing power iso	1.158	1.113	—	—
Mean FoM			0.277	—
Refinement				
Resolution range	—	—	20–3.0	20–2.5
Reflections (test set)	—	—	11819 (638)	20825 (1146)
R_{work}	—	—	0.205	0.216
R_{free}	—	—	0.251	0.265
No. of atoms	—	—	2731	2788
rmsd bonds, Å	—	—	0.012	0.012
rmsd angles, °	—	—	1.384	1.294
Ramachandran plot [†]				
% most favored region	—	—	88.7	91.8
% additionally allowed	—	—	11.0	8.2

*Values in parenthesis for outer shell.

[†]As defined in Procheck (1).1 Laskowski RA, MacArthur MW, Moss DS, Thornton JM (1993) PROCHECK: A program to check the stereochemical quality of protein structures. *J Appl Crystallogr* 26:283–291.